

**High-Performance Anthraquinone with Potentially Low Cost
for Aqueous Redox Flow Batteries**

Journal:	<i>Journal of Materials Chemistry A</i>
Manuscript ID	TA-ART-10-2021-008900.R1
Article Type:	Paper
Date Submitted by the Author:	12-Nov-2021
Complete List of Authors:	Wu, Min; Harvard School of Engineering and Applied Sciences Bahari, Meisam; Harvard University John A Paulson School of Engineering and Applied Sciences Fell, Eric; Harvard University, School of Engineering and Applied Sciences Gordon, Roy; Harvard University, Department of Chemistry and Chemical Biology Aziz, Michael; Harvard School of Engineering and Applied Sciences,

1 High-Performance Anthraquinone with Potentially
2 Low Cost for Aqueous Redox Flow Batteries

3 *Min Wu,¹ Meisam Bahari,¹ Eric M. Fell,¹ Roy G. Gordon,²*Michael J. Aziz¹**

4 ¹ John A. Paulson School of Engineering and Applied Sciences, Harvard University, Cambridge,
5 Massachusetts 02138, United States

6 ² Department of Chemistry and Chemical Biology, Harvard University, Cambridge,
7 Massachusetts 02138, United States

8 **Corresponding Author**

9 * gordon@chemistry.harvard.edu; * maziz@harvard.edu

10 ABSTRACT: Electrolyte cost and long-term durability are the two most challenging obstacles to
11 the practical utilization of redox-active organics in aqueous redox flow batteries. Starting from
12 potentially inexpensive 1,8-dihydroxyanthraquinone (1,8-DHAQ), we developed a one-pot, green,
13 and scalable approach to synthesize a highly water-soluble and potentially low-cost anthraquinone
14 1,8-dihydroxy-2,7-dicarboxymethyl-9,10-anthraquinone (DCDHAQ). The demonstrated
15 volumetric capacity of DCDHAQ in 1 M KOH is 40.2 Ah/L, which is around 70 times higher than
16 that of its precursor 1,8-DHAQ (0.567 Ah/L) at pH 14. The introduction of $-\text{CH}_2\text{CO}_2^-$ as
17 solubilizing groups suppressed the disproportionation reaction of reduced anthraquinone both
18 thermodynamically and kinetically. Consequently, the cycling stability of anthraquinone was
19 improved significantly compared to that of the precursor. Pairing a negolyte comprising 0.75 M
20 DCDHAQ with a posolyte comprising 0.3 M ferrocyanide at pH 14, we demonstrated a cell with
21 an open-circuit voltage of 1.1 V and a low capacity fade rate of 0.03%/day. The synthetic method
22 of attaching $-\text{CH}_2\text{CO}_2^-$ as solubilizing groups is likely applicable to other anthraquinone
23 derivatives and other aromatic organics as an inexpensive approach to performance enhancement
24 in energy applications.

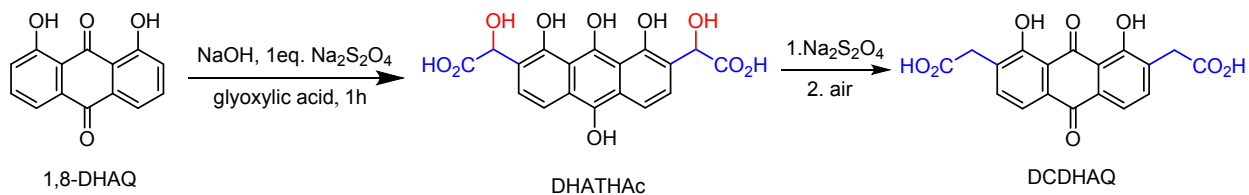
25

26 Bulk electrical energy storage technologies have attracted great attention because of their
27 capability to address the intrinsic intermittency of renewable energy sources such as solar and wind
28 electricity.¹⁻³ Aqueous redox-flow batteries are particularly attractive for grid-scale energy storage
29 owing to their flexible architecture, long cycle life, and good safety features.³ Aqueous vanadium
30 RFBs are the most commonly studied and adopted system, but their widespread application is
31 hindered by the availability and the fluctuating price of vanadium.²⁻⁴ In contrast, redox-active
32 organics comprising earth-abundant elements such as C, H, O, and N are potentially inexpensive
33 alternatives to vanadium.⁵⁻⁷ Redox-active organics based on quinone,⁸⁻²⁰ viologen,²¹⁻²⁹
34 phenazine,³⁰⁻³³ alloxazine,³⁴ and (2,2,6,6-tetramethylpiperidin-1-yl)oxyl^{21, 22, 30, 35-38} derivatives
35 have been studied for aqueous redox flow batteries. However, only a few anthraquinone,^{13, 18, 19}
36 phenazine,³³ and viologen^{24, 26, 27, 29} derivatives have demonstrated very good long-term stability;
37 others tend to have poor chemical stability. Viologens are vulnerable to attack by both protons and
38 hydroxide, making their practical implementation difficult, as a small amount of a side reaction,
39 e.g. with air leaking into the system, can lead to a large deviation from neutral pH.^{24, 29} Recently,
40 phenazine derivatives have also been reported to be extremely stable; however, they suffer from
41 high synthetic cost because expensive phenazine precursors, precious metal catalysts, and ligands
42 are used for the synthesis.³³ All of the extremely stable anthraquinones reported to date, such as
43 2,6-DBEAQ,¹³ 2,6-DPPEAQ,¹⁸ DPivOHAQ,^{19, 20} and DBAQ,^{19, 20} also suffer from high chemical
44 cost issues due to a multi-step synthesis or expensive precursors. Developing inexpensive, stable,
45 and soluble redox-active organics remains crucial for the practical implementation of aqueous
46 organic redox flow batteries (AORFBs).

47 Here, we report a potentially low-cost and highly soluble anthraquinone negolyte with good
48 cycling stability. The anthraquinone 1,8-dihydroxy-2,7-dicarboxymethyl-9,10-anthraquinone

49 (DCDHAQ) was synthesized from the relatively inexpensive precursor 1,8-
50 dihydroxyanthraquinone (1,8-DHAQ) with a one-pot, green synthesis method with water as the
51 solvent. The solubility of DCDHAQ at pH 14 is 1.3 M, which is almost two orders of magnitude
52 higher than that of its precursor 1,8-DHAQ (<0.02 M). The redox potential of DCDHAQ in 1M KOH
53 is -0.56 V vs. SHE; pairing with ferrocyanide, it enables a full cell voltage of 1.1 V. With this
54 simple $-\text{CH}_2\text{CO}_2^-$ functionalization, the average capacity fade rate decreases from 0.85%/day
55 for 1,8-DHAQ to as low as 0.03%/day for DCDHAQ. Moreover, the cost at mass-production scale
56 is estimated to be approximately \$6–8/kg (~\$40–50/kAh), depending on synthetic route, potentially
57 leading to a competitive flow battery chemistry. The inexpensive functionalization raises aqueous
58 solubility, decreases molecular crossover rates, and greatly increases the cycling stability of
59 anthraquinones, providing guidance for the rational design of redox-active organics for low cost
60 and ultra-stable cycling performance.

61 DCDHAQ was synthesized via a one-pot, green synthesis method with an inexpensive
62 precursor 1,8-DHAQ and finished in around 4 hours. As shown in **Scheme 1**, 1,8-DHAQ was
63 reduced by sodium dithionite. Subsequently, the side-chain precursor, glyoxylic acid, was added
64 to the solution, where the coupling reaction happened at room temperature to form 2,7-di-
65 hydroxyacetic acid-1,8,9,10-tetrahydroxy-anthracene (DHATHAc). DHATHAc was further
66 reduced with sodium dithionite and then air oxidized to form DCDHAQ.

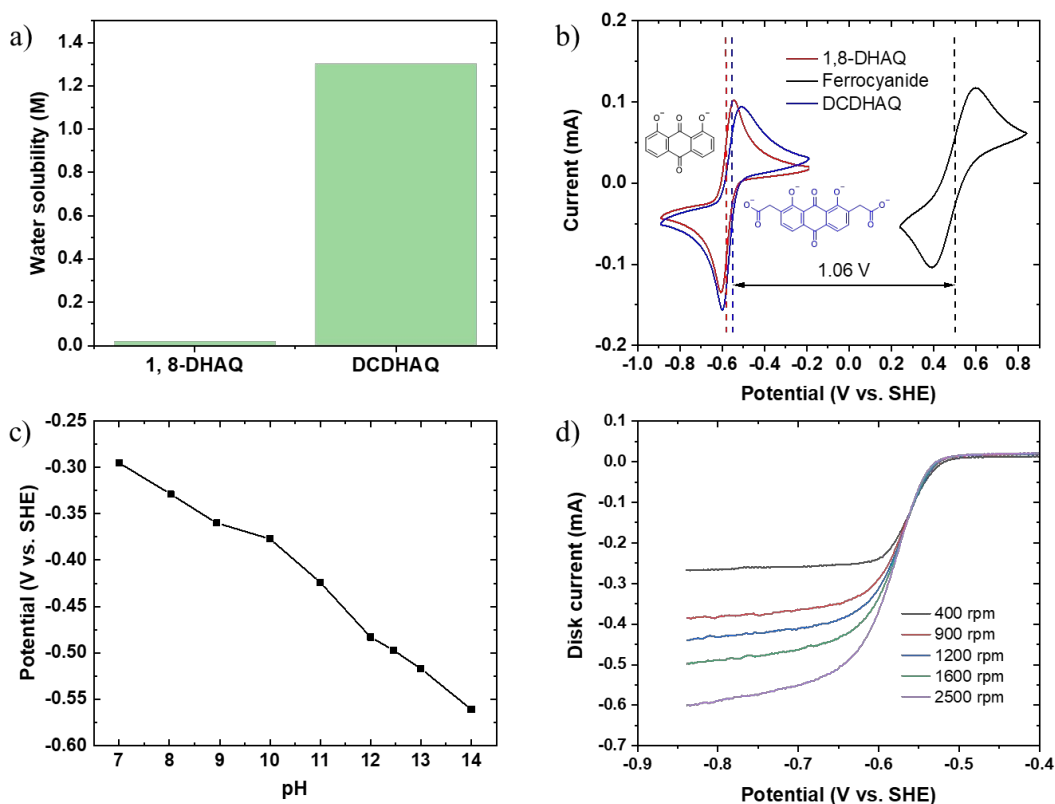


68 **Scheme 1.** Synthetic route for DCDHAQ.

69 **Figure 1a** compares the aqueous solubility of 1,8-DHAQ and DCDHAQ. 1,8-DHAQ has a
70 solubility of less than 0.02 M at pH 14, whereas DCDHAQ has a solubility of 1.3 M at pH 14,
71 corresponding to a volumetric capacity of 70 Ah/L. Thus, the volumetric capacity of anthraquinone
72 increased by more than one order of magnitude with a simple chemical functionalization. The
73 cyclic voltammograms (CV) of 1,8-DHAQ, DCDHAQ, and potassium ferrocyanide are shown in
74 **Figure 1b**. The redox potential of DCDHAQ at pH 14 is -0.56 V vs. SHE, which is 20 mV more
75 positive than that of 1,8-DHAQ. The increased redox potential of anthraquinone is known to
76 suppress the disproportionation side reaction of reduced anthraquinone thermodynamically,³⁹
77 thereby greatly increasing the cell cycling stability while slightly decreasing the cell voltage.
78 Additionally, DCDHAQ has two additional negative charges compared to 1,8-DHAQ, which
79 decrease the molecular crossover rate; the Coulomb repulsion also suppresses the rate of the
80 disproportionation side reaction, thereby increasing the cell lifetime.^{39,40} Pairing a DCDHAQ
81 negolyte with a potassium ferri/ferrocyanide posolyte at pH 14 yields an equilibrium cell potential
82 of approximately 1.06 V (**Figure 1b**). The Pourbaix diagram of DCDHAQ redox is shown in
83 **Figure 1c**. Unlike most anthraquinones, which exhibit a constant redox potential for pH exceeding
84 ~12, the redox potential of DCDHAQ continues to decrease as pH increases up to 14. Such
85 behavior is also observed in 1,8-dihydroxyanthraquinone.¹² The addition of 1,8-dihydroxy- groups
86 adds two additional pKas to the reduced anthraquinone, thereby increasing the final pKa of reduced
87 anthraquinone from 12 to beyond 14. As the posolyte redox potential is pH-independent, a higher
88 cell pH affords a higher full-cell voltage. The electrochemical properties of DCDHAQ were
89 determined by rotating disk electrode (RDE) measurement as shown in **Figure 1d**. The diffusion
90 coefficient of DCDHAQ was calculated by the Levich equation:

$$91 \quad i_L = 0.620nFAD^{\frac{2}{3}}\omega^{\frac{1}{2}}\nu^{-\frac{1}{6}}C \quad (1)$$

92 where i_L is the limiting current (mA) from the RDE test, n is the number of electrons transferred
 93 in the redox reaction, F is Faraday's constant (C/mol), A is the electrode area (cm²), D is the
 94 diffusion coefficient (cm²/s), ω is the angular rotation rate of the electrode (rad/s), ν is the
 95 kinematic viscosity (cm²/s), and C is the analyte concentration (mol/L). Based on the slope of the
 96 linear i_L vs. $\omega^{1/2}$ curve in **Figure S3a**, D is 1.7×10^{-6} cm² s⁻¹, which is similar to values reported for
 97 other redox organics in aqueous condition.⁴¹ The charge transfer coefficient was determined to be
 98 0.54 based on the Tafel equation, and the electron transfer rate constant was determined to be 7.4
 99 $\times 10^{-4}$ cm s⁻¹. The kinetic current was determined at different overpotentials by the *Koutecký*-
 100 *Levich* plot as shown in **Figure S4b**.



101

102

103 **Figure 1.** a) Solubility comparison for 1,8-DHAQ and DCDHAQ in 1 M KOH; b) Cyclic
 104 voltammograms of 5 mM 1,8-DHAQ, 5 mM DCDHAQ and 10 mM potassium ferrocyanide at pH
 105 14 with a scan rate of 100 mV/s; c) Pourbaix diagram of DCDHAQ redox process; d) Linear sweep

106 voltammograms of 5 mM DCDHAQ in 1 M KOH on a rotating disk electrode at rotation rates
107 between 400 and 2500 rpm.

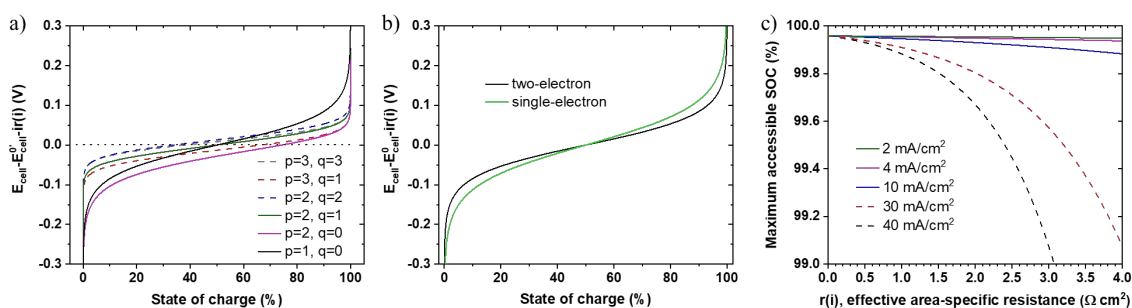
108 Capacity fade rate measurements with long-lived redox-active species are difficult because
109 very low fade rates can be obscured by a capacity measurement artifact caused by a temporal
110 variation in the cell resistance, e.g. from temperature drifts or membrane aging. To understand
111 how to minimize the sensitivity of measurements of apparent capacity, i.e the accessible state of
112 charge (SOC) range, to such artifacts, we performed a numerical simulation of SOC with effective
113 Nernstian voltage $E_{cell} - E_{cell}^{0'} - ir(i)$ for an anthraquinone capacity-limited or a capacity-
114 balanced cell. Here E_{cell} is the potential applied to the cell, SOC is the fraction of all anthraquinones
115 that is reduced, $E_{cell}^{0'}$ is the formal redox potential difference between posolyte and negolyte when
116 each is 50% reduced, $ir(i)$ is the overall cell overpotential including ohmic overpotential, mass
117 transport overpotential, and activation overpotential. And $r(i)$ is the effective, potentially nonlinear
118 area-specific resistance accounting for all overpotentials. Thus $E_{cell} - E_{cell}^{0'} - ir(i)$ is an effective
119 Nernstian voltage arising only from the relative concentrations of all the species in the two
120 electrolytes. It should be noted that the simulation applies to both charge/discharge processes; in
121 the charge process, i takes a positive value, while in the discharge process, i takes a negative value.
122 With the assumptions that the anthraquinone composing the negolyte undergoes a two-electron
123 redox process with both electron reduction potentials very close together, the ferrocyanide
124 composing the posolyte undergoes a one-electron redox process, no irreversible electrochemical
125 reactions are present, the activity coefficients are concentration-independent, and there is no
126 complex formation among the species, the Nernst equation yields

$$127 \quad E_{cell} = E_{cell}^{0'} + ir(i) + \frac{RT}{2F} \ln \left(\frac{SOC}{1-SOC} \times \left(\frac{q+SOC}{p-SOC} \right)^2 \right) \quad (2)$$

128 where R is the universal gas constant; T is the absolute temperature; F is Faraday's constant; and
129 p and q represent the initial charge capacity ratio of ferrocyanide to total anthraquinone (oxidized
130 plus reduced) and of ferricyanide to total anthraquinone, respectively (see supporting information
131 for calculation details). The relationship between effective Nernstian voltage $E_{cell} - E_{cell}^{0'} - ir(i)$
132 and the SOC is plotted in **Figure 2a**. It is clear that, to achieve an essentially full SOC, the
133 magnitude of $E_{cell} - E_{cell}^{0'} - ir(i)$ should be 0.2 V or above, especially for a capacity balanced cell
134 ($p=1, q=0$). Therefore, charging of the cell should be continued until the cell voltage is at least 0.2
135 V higher than $E_{cell}^{0'}$ for a two-electron redox molecule. **Figure 2b** compares the dependence of
136 $E_{cell} - E_{cell}^{0'} - ir(i)$ on SOC for a single-electron process in the posolyte and either a single-electron
137 process or a two-electron process in the negolyte, suggesting that, other things being equal,
138 accessing the same SOC requires charging to a higher cell voltage for a single-electron molecule
139 than for a two-electron molecule.

140 A common method of investigating charge capacity and its fade rate is to charge the cell to a
141 certain voltage (either potentiostatically or galvanostatically with a cutoff voltage), and then to
142 hold at that voltage until the current density decays to a fixed cutoff value before switching polarity
143 – and likewise for discharging. To investigate the relationship between maximum accessible SOC
144 and cut-off current density, we present **Figure 2c**, in which $r(i)$ is the effective area-specific
145 resistance (potentially non-constant) accounting for all overpotentials over the entire SOC range.
146 At intermediate SOC the activation overpotential has been shown to be Ohmic for species with
147 fast kinetics and the mass transport overpotential has been shown to be Ohmic for reactant
148 utilization (the fraction of reactant converted by the device in a single pass, which is proportional
149 to the current divided by the product of reactant concentration and flow rate) up to about 40%.^{42,43}

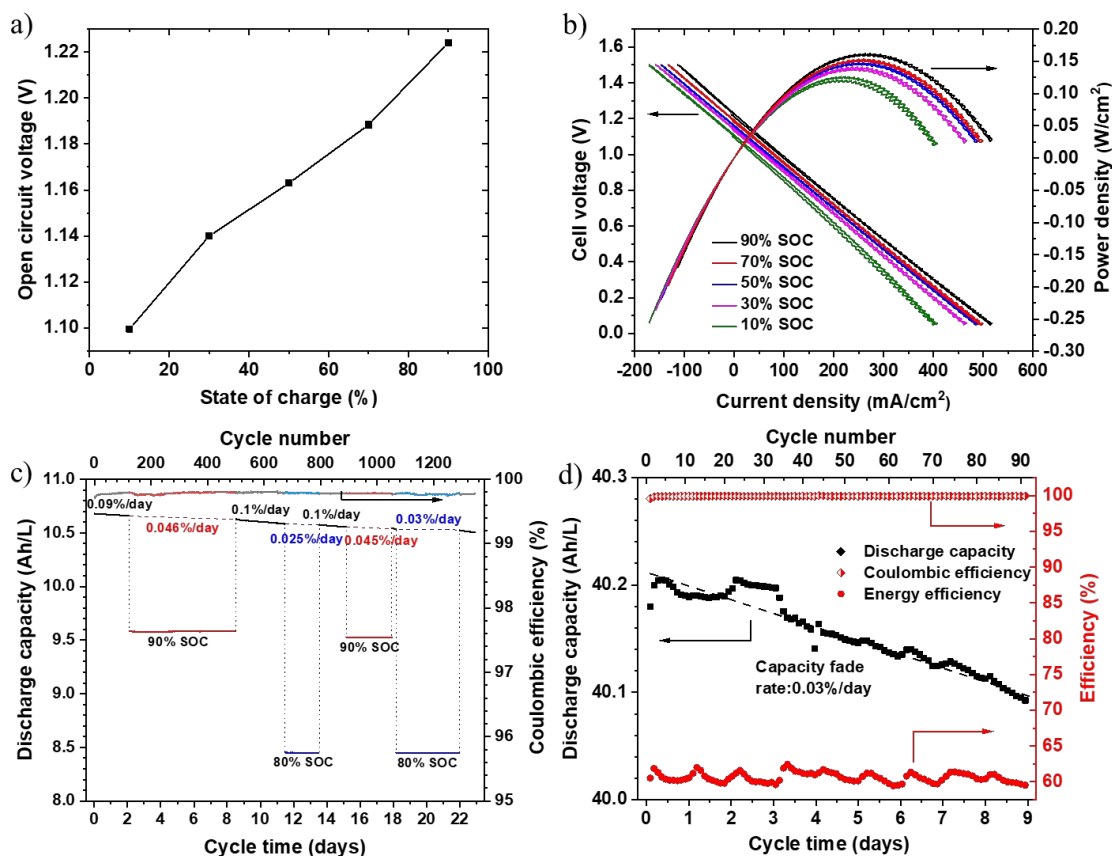
150 It is apparent from **Figure 2c** that, for current densities of tens of mA cm^{-2} , a small change in cell
 151 resistance, e.g through aging or temperature drifts, leads to a significant change in maximum
 152 accessible SOC, leading to large fluctuations in apparent cell capacity and the inability to evaluate
 153 low capacity fade rates. For a cell with a non-Ohmic mass transport overpotential, which may
 154 occur when the charging approaches the high-SOC limit where the concentration of available
 155 reactant becomes quite small and the utilization may become quite high, the mass transport
 156 overpotential increases superlinearly with current density.⁴³ The net effect of this nonlinear
 157 behavior is a move to the right along the curve for the current density under consideration. In other
 158 words, the assumption of Ohmic behavior in **Figure 2c** means that the curves represent an upper
 159 limit to the maximum accessible SOC. We conclude that, in order to measure stable high SOC
 160 values not subject to artifacts from drifting cell resistance, a potential hold until the current density
 161 drops to a small cut-off value is needed, as shown experimentally by Goulet and Aziz.⁴⁴ The
 162 simulation presented here serves as a guide for selecting numerical values of cycling voltage limits
 163 and cut-off current density for an accurate evaluation of discharge capacity and of slow capacity
 164 fade rates in redox flow batteries.



165

166 **Figure 2.** Simulations for a cell with a capacity-limiting negolyte and a posolyte comprising one-
 167 one-electron redox molecules. a) Calculated effective Nernstian voltage vs. SOC for negolyte
 168 comprising two-electron redox molecules of different electrolyte compositions; b) Calculated
 169 effective Nernstian voltage as a function of SOC for a capacity balanced cell ($p=1, q=0$) with
 170 negolyte undergoing a two-electron reaction or a single-electron reaction; c) Maximum accessible
 171 SOC vs. cell resistance for various cut-off current densities when $E_{cell} - E_{cell}^0 - ir(i)$ for a
 172 capacity-balanced cell ($p=1, q=0$) with negolyte comprising two-electron redox molecules.

173 Polarization experiments of a 0.75 M DCDHAQ/ferrocyanide full cell at pH 14 were
174 performed at various states of charge. The electrolytes comprised 5 mL of 0.75 M DCDHAQ
175 (negolyte) at pH 14 (0.75 M H₄DCDHAQ combined with 2 M KOH and 2 M NaOH) and 40 mL
176 of 0.3 M potassium ferrocyanide, 0.3 M potassium ferricyanide (posolyte) and 2 M NaCl at pH 14
177 (1M KOH) to ensure that the negolyte always remained the capacity limiting side during both
178 charging and discharging. We used mixed cations in the posolyte to raise the ferrocyanide
179 solubility. To reduce the osmotic imbalance, NaOH and KOH were used in the DCDHAQ negolyte
180 and NaCl was introduced into the posolyte. The concentrations were chosen such that the cation
181 concentrations were balanced at intermediate SOC. The cell was constructed from graphite flow
182 plates and AvCarb carbon cloth electrodes, separated by a Nafion 212 membrane pretreated in 1M
183 KOH to avoid changing the pH of the electrolytes. The carbon electrode was untreated and used
184 directly in all cell measurements, as commercial AvCarb carbon cloth is hydrophilic. To determine
185 its initial capacity, the cell was first charged and discharged galvanostatically with a potential hold
186 at 1.5 and 0.65 V, respectively, until the current density dropped to 2 mA/cm². Then, the cell was
187 charged to different SOC to measure the open-circuit voltage (OCV). The OCV increases from 1.1
188 to 1.23 V as the SOC increases from 10% to ~90% (**Figure 3a**). The OCV at 50% SOC is
189 approximately 1.16 V. A peak galvanic power density of 0.16 W cm⁻² was achieved at ~90% SOC
190 (**Figure 3b**). The power density may be increased by engineering improvements such as the
191 incorporation of lower-resistance membranes.



192

193 **Figure 3.** a) Open circuit voltage of 0.75 M DCDHAQ/0.3 M potassium ferrocyanide + 0.3 M
 194 potassium ferricyanide full cell at pH 14; b) Polarization measurements of the corresponding 0.75
 195 M full cell at pH 14; c) Cell cycling of 5 mL 0.2 M DCDHAQ and 30 mL 0.2 M ferrocyanide +
 196 0.02 M ferricyanide at pH 14; d) Discharge capacity, Coulombic efficiency, and round-trip energy
 197 efficiency during cycling of 0.75 M DCDHAQ with 0.3 M potassium ferrocyanide and 0.3 M
 198 potassium ferricyanide full cell at pH 14.

199 Long-term galvanostatic cycling of the 0.2 M DCDHAQ/ferrocyanide cell was performed at
 200 50 mA cm⁻² with potential holds at 1.4 V for charging and 0.8 V for discharging until the current
 201 density dropped to 2 mA cm⁻² (**Figure 3c**). The electrolytes comprised 5 mL of 0.2 M DCDHAQ
 202 (negolyte) at pH 14 and 40 mL of 0.2 M potassium ferrocyanide + 0.02 M potassium ferricyanide
 203 (posolyte) at pH 14. The initial discharge capacity at full SOC was 10.67 Ah L⁻¹ (theoretical value
 204 10.72 Ah L⁻¹). After 2.1 days of full SOC range cycling, the capacity faded by 0.19%,
 205 corresponding to a temporal capacity fade rate of 0.09%/day or 0.0017%/cycle. We expect fade

206 rates measured this way in full cells to provide upper limits on true molecular decomposition rates
207 because of the possible contribution of molecular crossover. For the next 6.4 days, the cell
208 continued to be charged galvanostatically to 90% SOC at 50 mA cm⁻² and immediately discharged
209 to 0.8 V at 50 mA cm⁻² with a potential hold, until the current density dropped to 2 mA cm⁻². The
210 cell was subsequently charged back to full SOC to evaluate the capacity fade rate during cycling
211 when charging had been limited to 90% SOC. The capacity fade rate when charging was limited
212 to 90% SOC was determined to be 0.046%/day or 0.00074%/cycle. Similarly, the average capacity
213 fade rate when charging was limited to 80% SOC was around 0.03%/day. The increased cycling
214 stability at lower charge-limiting SOC suggests that the capacity fade was due to the formation of
215 electrochemically inactive anthrone, which is known to be suppressed by limiting charging during
216 cycling.³⁹ Cycling was continued at different limiting SOC's (100%, 90%, 100%, 80%, 100%, 90%,
217 100%, 80%, 100%) for 23 days, and the discharge capacity was always determined immediately
218 after fully charging the cell. The average capacity fade rate for the 23 days of cycling was
219 0.068%/day or 0.0011%/cycle with an average coulombic efficiency of 99.8%. As shown in Table
220 S1, which excludes results from molecules requiring multiple synthetic steps or expensive
221 precursors, this stands out as the most stable cell performance to date with potentially low-cost
222 redox-active organic molecules.

223 Long-term cycling of the 0.75 M DCDHAQ/ferrocyanide cell was performed at 40 mA cm⁻²
224 with potential holds at 1.5 V for charging and 0.65 V for discharging until the current density
225 dropped to 2 mA cm⁻² (**Figure 3d**). The composition and volumes of the electrolytes are the same
226 as those in the polarization experiment. It should be noted that the great excess of posolyte used
227 here keeps the state of charge in the posolyte relatively invariant and prevents the posolyte from
228 becoming capacity limiting, thereby enabling the accurate determination of the negolyte capacity

229 fade rate. In practical deployment, such an excess is unnecessary. The wide voltage window and
230 low cut-off current density applied here should access the full cell capacity, according to the
231 simulation results presented in **Figure 2**. When the cut-off voltage with respect to the measured
232 OCV and the cut-off current density are appropriate as the simulations suggest, measurements of
233 capacity and true capacity fade rate reflect losses from chemical decomposition, leakage, or
234 crossover of active species from the capacity limiting side.⁴⁵ The initial volumetric capacity was
235 40.2 Ah L⁻¹, which is equal to the theoretical capacity. The measured volumetric capacity is one
236 of the highest capacities demonstrated experimentally for AORFBs.^{14,17} The coulombic efficiency
237 is above 99.9% over the whole cycling process. Although the round-trip energy efficiency exhibits
238 large fluctuations in **Figure 3d** due to daily temperature oscillations in the laboratory, the daily
239 capacity fluctuation was much smaller; this highlights the importance of the potential-hold method
240 to accurately evaluate the capacity fade rate. After 9 days of cycling, the volumetric capacity faded
241 by 0.27%, which corresponded to a temporal capacity fade of 0.03%/day, or 0.0029%/cycle,
242 representing one of the most stable organics reported.³ The DCDHAQ electrolytes before and after
243 cycling were analyzed with ¹H NMR. As shown in **Figure S5**, no apparent chemical
244 decomposition was observed, indicating the high chemical stability of DCDHAQ molecule.

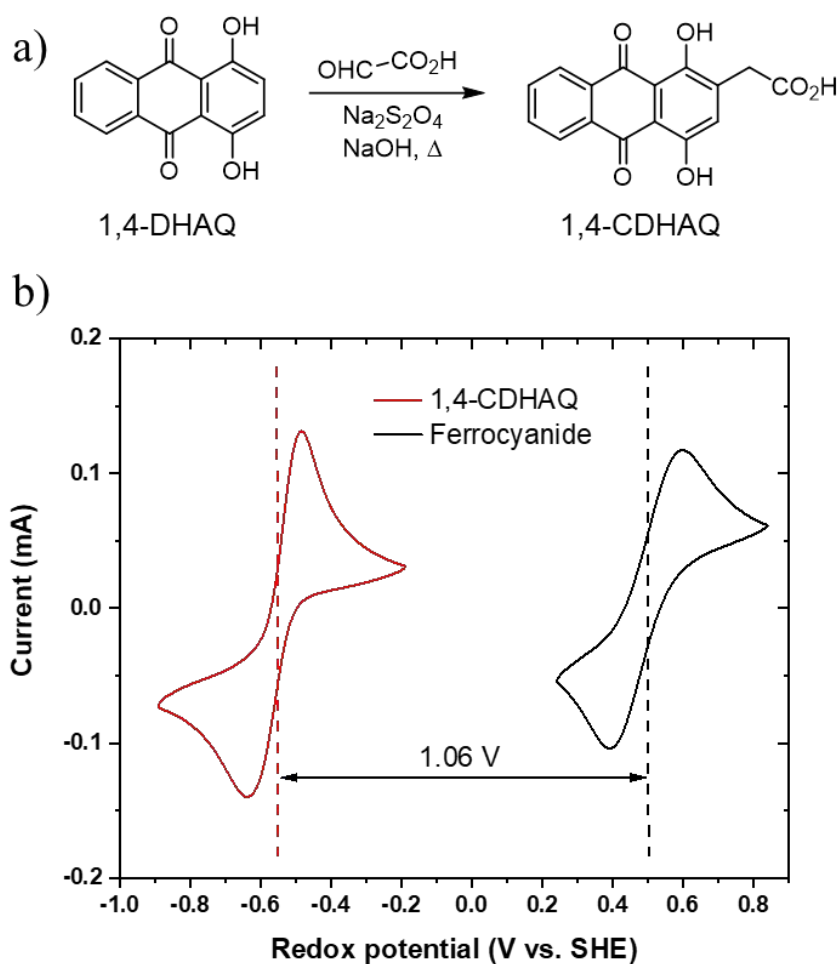
245 For comparison, a 1,8-DHAQ/ferrocyanide full cell was cycled at pH 14. The negolyte
246 consisted of 6 mL saturated 1,8-DHAQ at pH 14 (1M KOH) and the posolyte consisted of 30 mL
247 0.1 M potassium ferrocyanide and 0.02 M potassium ferricyanide at pH 14 (1 M KOH). The
248 membrane was Nafion 212, and the electrode was untreated AvCarb carbon electrodes, as in the
249 DCDHAQ/ferrocyanide cell. The cell was cycled between 0.8-1.4 V with a potential hold until the
250 current dropped to 2 mA/cm². The initial volumetric capacity for the saturated 1,8-DHAQ at pH
251 14 was 0.567 Ah/L as shown in **Figure S6**, which is less than 2% of the demonstrated volumetric

252 capacity in the DCDHAQ cell. The cell lost 2% of its capacity in the first half day, and then the
253 capacity fade rate decayed to around 0.85%/day, which is much higher than that of DCDHAQ cell
254 at 0.2 M (0.09%/day) and 0.75 M concentration (0.03%/day). Overall, the introduction of two
255 $-\text{CH}_2\text{CO}_2\text{H}$ groups not only increases the volumetric capacity but also greatly increases the
256 anthraquinone lifetime.

257 When considering the potential for practical deployment, the electrolyte cost at a commercial
258 scale is one of the most important factors but is also one of the most difficult to assess for a new
259 composition of matter. The laboratory-scale cost of the precursor 1,8-DHAQ is low compared to
260 that of its isomer 2,6-DHAQ, as shown in **Table S2** (see Estimated Cost of Electrolytes in the
261 Supporting Information). Given that DCDHAQ synthesis is a one-pot green method that uses water
262 as the solvent and inexpensive glyoxylic acid as the chain precursor, its synthetic cost at a
263 commercial scale should be low. Additionally, the reaction should also proceed with an
264 electrochemical synthesis method such as that shown in **Figure S7**, which would avoid the use of
265 sodium dithionite. As discussed in the Supporting Information, the mass-production cost of
266 DCDHAQ is estimated to be approximately \$8 – 10.4/kg by the chemical synthetic route reported
267 here and between \$6–8/kg by the electrochemical synthetic route.

268 To demonstrate the generality of the synthetic method of attaching glyoxylic acid groups, we
269 attached a single $-\text{CH}_2\text{COOH}$ group to 1,4-DHAQ, forming 1,4-dihydroxy-2-carboxymethyl-
270 9,10-anthraquinone (1,4-CDHAQ), as shown in Figure 4. Compared to DCDHAQ, the mass-
271 production cost of 1,4-CDHAQ may be lower because of the lower cost of 1,4-DHAQ (Table S2)
272 and the use of only half as much of the chain precursor as for DCDHAQ. 1,4-DHAQ is readily
273 produced from phthalic anhydride and 4-chlorophenol; thus, it is the least expensive of the DHAQ

274 family with a cost comparable to that of anthraquinone.⁴⁶ The solubility at pH 14 of 1,4-CDHAQ
275 is 1.0 M, corresponding to a volumetric capacity of 53.6 Ah/L, which is more than 10 times that
276 of 1,4-DHAQ (**Figure S8**) and comparable to that of DCDHAQ. The redox potential of 1,4-
277 CDHAQ is -0.56 V vs. SHE at pH 14, enabling it to form a 1.05 V full cell when paired with
278 potassium ferrocyanide (Figure 4b). Unfortunately, 1,4-CDHAQ appears, based on color changes
279 in **Figure S9** and current decreases in CV results in **Figure S10**, to react irreversibly with
280 ferricyanide. The irreversible decomposition is tentatively attributed to the oxidation of 1,4-
281 hydroxy groups in 1,4-CDHAQ by ferricyanide, followed by Michael addition. A similar
282 decomposition mechanism has been observed in both alizarin and quinizarin derivatives at high
283 oxidation potential.⁴⁷ Since the crossover of ferricyanide cannot be avoid in Nafion 212 membrane,
284 thus cell-scale performance evaluation of 1,4-CDHAQ must await a membrane with a negligible
285 ferricyanide crossover rate and not evaluated here.



286

287 **Figure 4.** a) Synthetic route for 1,4-CDHAQ; b) Cyclic voltammograms of 5 mM 1,4-CDHAQ
288 and 10 mM potassium ferrocyanide at pH 14 with a scan rate of 100 mV/s.

289 We showed how simple molecular modification of a potentially inexpensive but poorly-
290 performing aromatic precursor can improve the performance of redox-active organics in aqueous
291 flow batteries. We demonstrated a high-performance AORFB with a highly soluble, stable, and
292 potentially inexpensive anthraquinone in the negolyte. Because glyoxylic acid is known to react
293 with phenol,⁴⁸ the potentially inexpensive synthetic method of attaching glyoxylate groups on
294 aromatics might be readily extended to other anthraquinone derivatives and perhaps other
295 aromatics, accelerating the development of redox-active organics for practical application. Finally,
296 the simulated results relating SOC to cycling voltage limits and cut-off current density provide
297 quantitative guidance for accurate evaluation of cell capacity and its fade rate.

298 ASSOCIATED CONTENT

299 **Supporting Information.** The Supporting Information is available free of charge at

300 Figures S1–S10; Tables S1, S2; and detailed descriptions on the DCDHAQ and 1,4-

301 CDHAQ synthesis, estimation of electrolyte cost, discussion of the relationship between state of

302 charge, cut-off voltage and cell current.

303 AUTHOR INFORMATION

304 **Corresponding authors**

305 * Roy G. Gordon: Dept. of Chemistry and Chemical Biology, Harvard University, 12 Oxford
306 Street, MA 02138. E-mail: gordon@chemistry.harvard.edu.

307 * Michael J. Aziz: John A. Paulson School of Engineering and Applied Sciences, Harvard
308 University, Pierce Hall 204a, 29 Oxford Street, MA 02138. E-mail: maziz@harvard.edu.

309 **ORCID[®]**

310 Min Wu: <https://orcid.org/0000-0002-1742-1966>

311 Meisam Bahari: <https://orcid.org/0000-0002-5800-3349>

312 Eric M. Fell: <https://orcid.org/0000-0003-2046-1480>

313 Roy G. Gordon: <https://orcid.org/0000-0001-5980-268X>

314 Michael J. Aziz: <https://orcid.org/0000-0001-9657-9456>

315

316 **Conflict of Interest Statement**

317 M.J.A. and M.B. have an ownership stake in Quino Energy, Inc., which may profit from the

318 materials reported herein.

319 **ACKNOWLEDGMENT**

320 This research was supported by U.S. DOE award DE-AC05-76RL01830 through PNNL

321 subcontract 535264 and Innovation Fund Denmark via the Grand Solutions project "ORBATS"

322 file no. 7046-00018B. The authors thank Dr. Eugene Beh, Dr. Yan Jing, Martin Jin, Emily Kerr,

323 Daniel Pollack, and Jinxu Gao for valuable discussions.

324 REFERENCES

- 325 1. Dunn, B.; Kamath, H.; Tarascon, J.-M., Electrical Energy Storage for the Grid: A Battery
326 of Choices. *Science* **2011**, *334*, 928-935.
- 327 2. Soloveichik, G. L., Flow Batteries: Current Status and Trends. *Chem Rev* **2015**, *115* (20),
328 11533-58.
- 329 3. Kwabi, D. G.; Ji, Y.; Aziz, M. J., Electrolyte lifetime in aqueous organic redox flow
330 batteries: A critical review. *Chem Rev* **2020**, *120* (14), 6467–6489.
- 331 4. Darling, R. M.; Gallagher, K. G.; Kowalski, J. A.; Ha, S.; Brushett, F. R., Pathways to
332 low-cost electrochemical energy storage: a comparison of aqueous and nonaqueous flow
333 batteries. *Energy & Environmental Science* **2014**, *7* (11), 3459-3477.
- 334 5. Wei, X. L.; Pan, W. X.; Duan, W. T.; Hollas, A.; Yang, Z.; Li, B.; Nie, Z. M.;
335 Liu, J.; Reed, D.; Wang, W.; Sprenkle, V., Materials and Systems for Organic Redox Flow
336 Batteries: Status and Challenges. *ACS Energy Letters* **2017**, *2* (9), 2187-2204.

- 337 6. Luo, J. A.; Hu, B.; Hu, M. W.; Zhao, Y.; Liu, T. L., Status and Prospects of Organic
338 Redox Flow Batteries toward Sustainable Energy Storage. *ACS Energy Letters* **2019**, *4* (9),
339 2220-2240.
- 340 7. Brushett, F. R.; Aziz, M. J.; Rodby, K. E., On lifetime and cost of redox-active organics
341 for aqueous flow batteries. *ACS Energy Letters* **2020**, *5*, 879-884.
- 342 8. Huskinson, B. T.; Marshak, M. P.; Suh, C.; Er, S.; Gerhardt, M. R.; Galvin, C. J.;
343 Chen, X.; Aspuru-Guzik, A.; Gordon, R. G.; Aziz, M. J., A metal-free organic-inorganic
344 aqueous flow battery. *Nature* **2014**, *505* (7482), 195-8.
- 345 9. Lin, K.; Chen, Q.; Gerhardt, M. R.; Tong, L.; Kim, S. B.; Eisenach, L.; Valle, A.
346 W.; Hardee, D.; Gordon, R. G.; Aziz, M. J.; Marshak, M. P., Alkaline quinone flow battery.
347 *Science* **2015**, *349* (6255), 1529-32.
- 348 10. Gerhardt, M. R.; Tong, L.; Gomez-Bombarelli, R.; Chen, Q.; Marshak, M. P.;
349 Galvin, C. J.; Aspuru-Guzik, A.; Gordon, R. G.; Aziz, M. J., Anthraquinone Derivatives in
350 Aqueous Flow Batteries. *Advanced Energy Materials* **2017**, *7* (8), 1601488.

- 351 11. Yang, Z.; Tong, L.; Tabor, D. P.; Beh, E. S.; Goulet, M. A.; De Porcellinis, D.;
352 Aspuru-Guzik, A.; Gordon, R. G.; Aziz, M. J., Alkaline Benzoquinone Aqueous Flow Battery
353 for Large-Scale Storage of Electrical Energy. *Advanced Energy Materials* **2018**, *8*(8), 1702056.
- 354 12. Cao, J. Y.; Tao, M.; Chen, H. P.; Xu, J.; Chen, Z. D., A highly reversible
355 anthraquinone-based anolyte for alkaline aqueous redox flow batteries. *Journal of Power Sources*
356 **2018**, *386*, 40-46.
- 357 13. Kwabi, D. G.; Lin, K.; Ji, Y.; Kerr, E. F.; Goulet, M.-A.; De Porcellinis, D.;
358 Tabor, D. P.; Pollack, D. A.; Aspuru-Guzik, A.; Gordon, R. G.; Aziz, M. J., Alkaline
359 quinone flow battery with long lifetime at pH 12. *Joule* **2018**, *2*(9), 1907-1908.
- 360 14. Jin, S.; Jing, Y.; Kwabi, D. G.; Ji, Y.; Tong, L.; De Porcellinis, D.; Goulet, M.
361 A.; Pollack, D. A.; Gordon, R. G.; Aziz, M. J., A water-miscible quinone flow battery with
362 high volumetric capacity and energy density. *ACS Energy Letters* **2019**, *4*(6), 1342-1348.
- 363 15. Park, M.; Beh, E. S.; Fell, E. M.; Jing, Y.; Kerr, E. F.; De Porcellinis, D.; Goulet,
364 M. A.; Ryu, J.; Wong, A. A.; Gordon, R. G.; Cho, J.; Aziz, M. J., A High Voltage
365 Aqueous Zinc-Organic Hybrid Flow Battery. *Advanced Energy Materials* **2019**, *9*(25), 1900694.

- 366 16. Tong, L.; Goulet, M.-A.; Tabor, D. P.; Kerr, E. F.; De Porcellinis, D.; Fell, E. M.;
367 Aspuru-Guzik, A.; Gordon, R. G.; Aziz, M. J., Molecular Engineering of an Alkaline
368 Naphthoquinone Flow Battery. *ACS Energy Letters* **2019**, *4* (8), 1880-1887.
- 369 17. Hu, B.; Luo, J.; Hu, M.; Yuan, B.; Liu, T. L., A pH-Neutral, Metal-Free Aqueous
370 Organic Redox Flow Battery Employing an Ammonium Anthraquinone Anolyte. *Angew Chem*
371 *Int Ed* **2019**, *58* (46), 16629-16636.
- 372 18. Ji, Y.; Goulet, M. A.; Pollack, D. A.; Kwabi, D. G.; Jin, S.; Porcellinis, D.; Kerr,
373 E. F.; Gordon, R. G.; Aziz, M. J., A Phosphonate-Functionalized Quinone Redox Flow Battery
374 at Near-Neutral pH with Record Capacity Retention Rate. *Advanced Energy Materials* **2019**, *9*
375 (12), 1900039.
- 376 19. Wu, M.; Jing, Y.; Wong, A. A.; Fell, E. M.; Jin, S.; Tang, Z.; Gordon, R. G.;
377 Aziz, M. J., Extremely stable anthraquinone negolytes synthesized from common precursors.
378 *Chem* **2020**, *6*, 11.

- 379 20. Jing, Y.; Wu, M.; Wong, A. A.; Fell, E. M.; Jin, S.; Pollack, D. A.; Kerr, E. F.;
380 Gordon, R. G.; Aziz, M. J., In situ electrosynthesis of anthraquinone electrolytes in aqueous flow
381 batteries. *Green Chem* **2020**, *22* (18), 6084-6092.
- 382 21. Liu, T. B.; Wei, X. L.; Nie, Z. M.; Sprenkle, V.; Wang, W., A Total Organic Aqueous
383 Redox Flow Battery Employing a Low Cost and Sustainable Methyl Viologen Anolyte and 4-
384 HO-TEMPO Catholyte. *Advanced Energy Materials* **2015**, *6* (3), 1501449.
- 385 22. Janoschka, T.; Morgenstern, S.; Hiller, H.; Friebe, C.; Wolkersdorfer, K.; Hauptler,
386 B.; Hager, M. D.; Schubert, U. S., Synthesis and characterization of TEMPO- and viologen-
387 polymers for water-based redox-flow batteries. *Polymer Chemistry* **2015**, *6* (45), 7801-7811.
- 388 23. Hu, B.; DeBruler, C.; Rhodes, Z.; Liu, T. L., Long-Cycling Aqueous Organic Redox
389 Flow Battery (AORFB) toward Sustainable and Safe Energy Storage. *J Am Chem Soc* **2017**, *139*
390 (3), 1207-1214.
- 391 24. Beh, E. S.; De Porcellinis, D.; Gracia, R. L.; Xia, K. T.; Gordon, R. G.; Aziz, M. J.,
392 A Neutral pH Aqueous Organic-Organometallic Redox Flow Battery with Extremely High
393 Capacity Retention. *ACS Energy Letters* **2017**, *2* (3), 639-644.

- 394 25. Luo, J.; Hu, B.; Debruler, C.; Liu, T. L., A pi-Conjugation Extended Viologen as a Two-
395 Electron Storage Anolyte for Total Organic Aqueous Redox Flow Batteries. *Angew. Chem. Int.*
396 *Ed.* **2018**, *57*(1), 231-235.
- 397 26. DeBruler, C.; Hu, B.; Moss, J.; Luo, J.; Liu, T. L., A Sulfonate-Functionalized
398 Viologen Enabling Neutral Cation Exchange, Aqueous Organic Redox Flow Batteries toward
399 Renewable Energy Storage. *ACS Energy Letters* **2018**, *3*(3), 663-668.
- 400 27. Liu, W.; Liu, Y.; Zhang, H.; Xie, C.; Shi, L.; Zhou, Y. G.; Li, X., A highly stable
401 neutral viologen/bromine aqueous flow battery with high energy and power density. *Chem.*
402 *Commun.* **2019**, *55*(33), 4801-4804.
- 403 28. Ohira, A.; Funaki, T.; Ishida, E.; Kim, J.-D.; Sato, Y., Redox-Flow Battery Operating
404 in Neutral and Acidic Environments with Multielectron-Transfer-Type Viologen Molecular
405 Assembly. *ACS Applied Energy Materials* **2020**, *3*(5), 4377-4383.
- 406 29. Jin, S.; Fell, E. M.; Vina-Lopez, L.; Jing, Y.; Michalak, P. W.; Gordon, R. G.;
407 Aziz, M. J., Near Neutral pH Redox Flow Battery with Low Permeability and Long-Lifetime
408 Phosphonated Viologen Active Species. *Advanced Energy Materials* **2020**, *10*(20), 2000100.

- 409 30. Winsberg, J.; Stolze, C.; Muench, S.; Liedl, F.; Hager, M. D.; Schubert, U. S.,
410 TEMPO/Phenazine Combi-Molecule: A Redox-Active Material for Symmetric Aqueous Redox-
411 Flow Batteries. *ACS Energy Letters* **2016**, *1* (5), 976-980.
- 412 31. Hollas, A.; Wei, X. L.; Murugesan, V.; Nie, Z. M.; Li, B.; Reed, D.; Liu, J.;
413 Sprenkle, V.; Wang, W., A biomimetic high-capacity phenazine-based anolyte for aqueous
414 organic redox flow batteries. *Nature Energy* **2018**, *3* (6), 508-514.
- 415 32. Wang, C.; Li, X.; Yu, B.; Wang, Y.; Yang, Z.; Wang, H.; Lin, H.; Ma, J.; Li,
416 G.; Jin, Z., Molecular Design of Fused-Ring Phenazine Derivatives for Long-Cycling Alkaline
417 Redox Flow Batteries. *ACS Energy Letters* **2020**, *5* (2), 411-417.
- 418 33. Pang, S.; Wang, X.; Wang, P.; Ji, Y., Biomimetic Amino Acid Functionalized Phenazine
419 Flow Batteries with Long Lifetime at Near-Neutral pH. *Angew. Chem. Int. Ed.* **2021**, *60*, 5289 –
420 5298
- 421 34. Lin, K.; Gomez-Bombarelli, R.; Beh, E. S.; Tong, L.; Chen, Q.; Valle, A.;
422 Aspuru-Guzik, A.; Aziz, M. J.; Gordon, R. G., A redox-flow battery with an alloxazine-based
423 organic electrolyte. *Nature Energy* **2016**, *1* (9), 16102.

- 424 35. Winsberg, J.; Janoschka, T.; Morgenstern, S.; Hagemann, T.; Muench, S.;
425 Hauffman, G.; Gohy, J. F.; Hager, M. D.; Schubert, U. S., Poly(TEMPO)/Zinc Hybrid-Flow
426 Battery: A Novel, "Green," High Voltage, and Safe Energy Storage System. *Adv. Mater.* **2016**,
427 *28* (11), 2238-43.
- 428 36. Chang, Z.; Henkensmeier, D.; Chen, R., One-Step Cationic Grafting of 4-Hydroxy-
429 TEMPO and its Application in a Hybrid Redox Flow Battery with a Crosslinked PBI Membrane.
430 *ChemSusChem* **2017**, *10* (16), 3193-3197.
- 431 37. Winsberg, J.; Stolze, C.; Schwenke, A.; Muench, S.; Hager, M. D.; Schubert, U. S.,
432 Aqueous 2,2,6,6-Tetramethylpiperidine-N-oxyl Catholytes for a High-Capacity and High
433 Current Density Oxygen-Insensitive Hybrid-Flow Battery. *ACS Energy Letters* **2017**, *2* (2), 411-
434 416.
- 435 38. Liu, Y. H.; Goulet, M. A.; Tong, L. C.; Liu, Y. Z.; Ji, Y. L.; Wu, L.; Gordon, R.
436 G.; Aziz, M. J.; Yang, Z. J.; Xu, T. W., A Long-Lifetime All-Organic Aqueous Flow Battery
437 Utilizing TMAP-TEMPO Radical. *Chem* **2019**, *5* (7), 1861-1870.

- 438 39. Goulet, M.-A.; Tong, L.; Pollack, D. A.; Tabor, D. P.; Odom, S. A.; Aspuru-Guzik,
439 A.; Kwan, E. E.; Gordon, R. G.; Aziz, M. J., Extending the lifetime of organic flow batteries
440 via redox state management. *J. Am. Chem. Soc.* **2019**, *141* (20), 8014-8019.
- 441 40. Hu, B.; Tang, Y.; Luo, J.; Grove, G.; Guo, Y.; Liu, T. L., Improved radical stability
442 of viologen anolytes in aqueous organic redox flow batteries. *Chem. Commun.* **2018**, *54* (50),
443 6871-6874.
- 444 41. Gharagheizi, F., Determination of Diffusion Coefficient of Organic Compounds in Water
445 Using a Simple Molecular-Based Method. *Industrial & Engineering Chemistry Research* **2012**,
446 *51* (6), 2797-2803.
- 447 42. Chen, Q., Gerhardt, M. R., & Aziz, M. J., Dissection of the voltage losses of an acidic
448 quinone redox flow battery. *Journal of The Electrochemical Society*, **2017**, *164*(6), A1126.
- 449 43. Wong, A. A.; Aziz, M. J., Method for Comparing Porous Carbon Electrode Performance in
450 Redox Flow Batteries. *Journal of The Electrochemical Society* **2020**, *167*, 110542.
- 451 44. Goulet, M. A.; Aziz, M. J., Flow battery molecular reactant stability determined by
452 symmetric cell cycling methods. *Journal of The Electrochemical Society*, **2018**, *165*(7), A1466.

- 453 45. Chen, Q.; Eisenach, L.; Aziz, M. J., Cycling Analysis of a Quinone-Bromide Redox Flow
454 Battery. *Journal of the Electrochemical Society* **2016**, *163* (1), A5057-A5063.
- 455 46. Bien, H.-S.; Stawitz, J.; Wunderlich, K., Anthraquinone Dyes and Intermediates. In
456 *Ullmann's Encyclopedia of Industrial Chemistry*, 2000.
- 457 47. Tong, L.; Jing, Y.; Gordon, R. G.; Aziz, M. J., Symmetric All-Quinone Aqueous Battery.
458 *ACS Applied Energy Materials* **2019**, *2* (6), 4016-4021.
- 459 48. Mattioda, G.; Christidis, Y., Glyoxylic Acid. In *Ullmann's Encyclopedia of Industrial*
460 *Chemistry*, 2000.
- 461